NANO LETTERS

2008
Vol. 8, No. 7
1971-1977

Assembly Pathway Analysis of DNA Nanostructures and the Construction of Parallel Motifs

Mudalige Thilak Kumara, Dmytro Nykypanchuk, and William B. Sherman*

P.O. Box 5000, Center for Functional Nanomaterials, Brookhaven National Laboratory, Upton, New York 11973

Received March 31, 2008; Revised Manuscript Received May 3, 2008

ABSTRACT

We present a system for analyzing the assembly pathway of DNA nanostructures. This enables the identification, explanation, and avoidance of obstacles to proper structure formation. Potential problems include strand end-pinning and misfolding caused by the structural bias of nominally flexible junctions. We have used this system to guide the construction of parallel motifs that had previously, for unknown reasons, resisted assembly.

Since Seeman first proposed structural DNA nanotechnology,[1] it has met with unprecedented success. Numerous branched DNA nanostructures have been developed,[2–31] which, in turn, have provided the foundation for mechanical[32–38] and enzymatic[39,40] nanodevices, chemical computation,[41–43] and the ordered assembly of nanoparticles,[44–46] proteins,[10,24,47,48] and other nanoscale guests.[49] Structural DNA nanotechnology derives much of its utility from the broad acceptance that a simple, geometry-based model allows the accurate prediction of what DNA structures can form.[50–52] We may be surprised by the behavior of some novel junction, base pairing, or reaction conditions, but within the realm of the familiar, theoretically sound structures are expected to assemble as planned. The archetypical DNA nanostructure is the double-crossover (DX),[4] consisting of two DNA domains connected by two immobile Holliday junctions.[53] Yet it is well-known within the field that of the five possible types of DX, first identified by Fu and Seeman, only two form well.[4] What is less well-appreciated is that the conventional theories provide no reason why. We present here an explanation based on analyzing the assembly and folding pathways of the DXs. We have used this analysis to design and cleanly assemble representatives of all three of the previously recalcitrant classes of DX.

Figure 1 shows the five classes of DX and explains the nomenclature used to refer to them. Initial experiments in the 5−10 μM range revealed that, of the five DXs, the DAEs and DAOs (collectively DAs) form well, while the DPEs, DPONs, and DPOWs (DPs) all assembled with substantial fractions in more than one species as observed by polyacrylamide gel electrophoresis (PAGE).[4] For systems with high-mass malformations, the yield of target DPs was raised as high as 90−95% by assembly at low concentrations (80−450 nM). No method was reported, however, for reducing the occurrence of ill-formed structures of mass similar to the

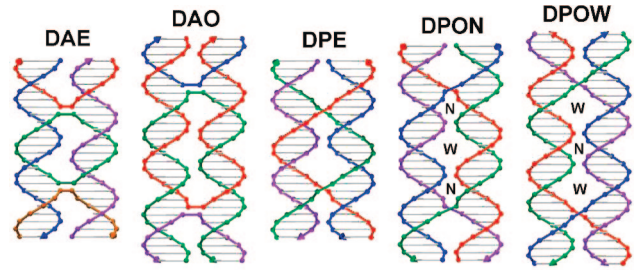

Figure 1. Five classes of DX isomer. The bases are represented by horizontal struts, and the backbones are shown in color with cones indicating the 3′ ends. The region between the junctions is the core, and the outer regions are referred to as the "arms". Each major DX class is identified by three or four letters. The first letter is always D for double-crossover. The second letter denotes the polarity of the junctions: A for antiparallel or P for parallel. In the antiparallel molecules, the red strands can be seen to progress down the left domain to a junction and then reverse directions and travel back up to the top of the right domain. In the parallel molecules, the red strands start at the bottom and proceed continuously upward, through one or two junctions, to the top of the molecule. The third letter specifies whether there are an even E or odd O number of strand crossings along one duplex domain in the core as viewed normal to the plane of the molecule. For antiparallel DXs (DAs), the inward grooves on the two duplexes are always opposite; for the parallel DXs (DPs), the inward grooves are always the same, either both major grooves inward or both minor grooves inward. Thus, there are DPOs with more narrow, minor grooves between junctions (DPONs) and DPOs with more wide, major grooves between junctions (DPOWs). DNA models drawn with GIDEON.[51]

* Corresponding author. E-mail: wsherman@bnl.gov.

10.1021/nl800907y CCC: $40.75
Published on Web 06/10/2008

target DPs. The study of DPs has been virtually abandoned in nanoscience, though a few biology-oriented studies have used ligation to assemble catenanes with DP crossover patterns.[54–62] The catenanes also form with an assortment of side products, but the target molecules are more easily purified and characterized than the standard DPs.[54,56]

The difficulties assembling DPs were not initially considered problematic for two main reasons. First, duplex domains connected via parallel junctions would have segments of their negatively charged phosphate backbones closely juxtaposed.[4] Second, it was well-known that individual Holliday junctions, while quite flexible, energetically favor an antiparallel configuration.[6,63,64] Either of these factors was thought an adequate explanation for why DPs are energetically unfavorable, and so the matter was largely laid to rest. Over the past decade, however, new experimental facts have arisen that refute these explanations.

In the late 1990s, paranemic crossovers (PXs) were accidentally discovered.[16,65] These structures are similar to DPs except that they have more parallel junctions. In 2006, triple crossover molecules with bow-tie junctions (TXBTs) were successfully constructed.[66] These structures have synthetic DNA oligomers that switch polarity as they pass between two of the duplexes. TXBTs have close backbone juxtapositions similar to those in DPs. The clean formation of PXs and the TXBTs demonstrated that both the parallel junctions and the backbone juxtapositions are energetically stable. While the significance of these developments went largely unnoted, the field was left in the difficult situation of not being able to explain why three of the five most fundamental structures would not form properly. This failure was particularly far reaching, since DXs are subcomponents of most of the DNA nanostructures developed to date, including such prominent examples as star motif arrays,[10–13] DNA nanotubes,[17–19,22–25,27,52] and DNA origami,[31] all of which were investigated solely using antiparallel junctions because of the early failures at constructing DPs.

Figure 2 shows a set of experiments that illustrates two different failure modes in the assembly of DPs, our analysis of the failures, and then a successful assembly. On the left side of the figure are sequence-structure diagrams of the three target molecules used. As much as possible, the sequences are identical; thus, the lower two molecules are truncated versions of the top molecule. Each target molecule is equally favorable according to geometrical modeling,[51] but their different assembly pathways ultimately dictate their success or failure at clean formation. The molecules are assembled by thermal annealing from 95 °C down to room temperature over about 12 h. Thus, their assembly pathway is a function of the thermal stability of the various sections of the molecules. The segments that have the highest melting temperatures are taken to hybridize first,[67] and, if they are not blocked, the segments with progressively lower melting temperatures will hybridize in turn. Next to the sequence-structure diagrams in Figure 2 are the melting temperatures for the various arms as estimated by HyTher™.[68,69] These indicate that the long, 12 base-pair (bp) arms have melting temperatures 10−16 °C higher than the medium length (10 bp) core sections, which, in turn, have melting temperatures 7−18 °C higher than the short arms (8 bp).

The central section of Figure 2 shows simple models illustrating, across each row, from left to right, the hypothesized states of the strands at decreasing temperatures while they are being annealed. In each case, the target molecule is shown at the right side, with the lengths of the core and the arms indicated as long (L), medium (M), or short (S), to suggest the order of assembly. This style of analysis highlights potential traps that the strands can fall into while they are being annealed. Thus, in the first two rows, we see on the right side possible misfolded structures as well as the target molecules. In the third row, only the target molecule, a DPE, is expected. The gel at the right confirms that the failure products and target molecules are running as predicted.

The top row of Figure 2 shows an instance of strand end-pinning.[52] This occurs when the ends of strands get structurally fixed, and block their middle sections from hybridizing together properly. In this case, the long arms hybridize before the medium length core sections as the system cools. This prevents the core from hybridizing without disrupting all of the base pairs in one of the arms. Some and possibly all of the molecules never hybridize completely but are trapped with a few bases topologically blocked from hybridizing. A possible example of such a state is shown above the target molecule in the top row of Figure 2. Such a misfolded structure is expected to run on a gel near the target structure. It remains unclear whether either of the split bands contains the properly folded DPE, though they both run at approximately the expected position of the target.

The second row of Figure 2 shows an example of junction-biased misfolding leading to multimerization. The target structure has short arms and medium length core sections. Thus, at the highest temperatures, the core sections hybridize. As the temperature lowers, the short arms start to become stable. However, as two such arms hybridize, a Holliday junction is formed,[53] which, under these conditions, favors the 63° antiparallel configuration shown in the middle of the row.[6] This junction resists the folding of the molecule into the target state. Two such Holliday junctions can join together into the structure shown at the top, right of the row. Larger chains of junctions can assemble, and that can explain the ladders of multimers previously observed for DPOs,[4] but the DPEs seem to dominantly form dimers, presumably because the structure shown cyclizes and thereby blocks the formation of larger multimers. In the second lane of the gel, we can see from the split upper band that runs at the same speed as the 130 bp band of the reference ladder that the DPE dimers can fold up at least two different ways. For such a dimer to form a quadrilateral, it needs to have at least two of its corners far from their 63° antiparallel relaxed state. This suggests that the split bands correspond to different pairs of strained junctions. The lower band of lane 2 runs at the expected rate of the target molecule.

Our hypothesis, confirmed in the right lane of the gel, is that a DPE will form cleanly if it avoids both the assembly problems of strand end-pinning and those of junction-biased

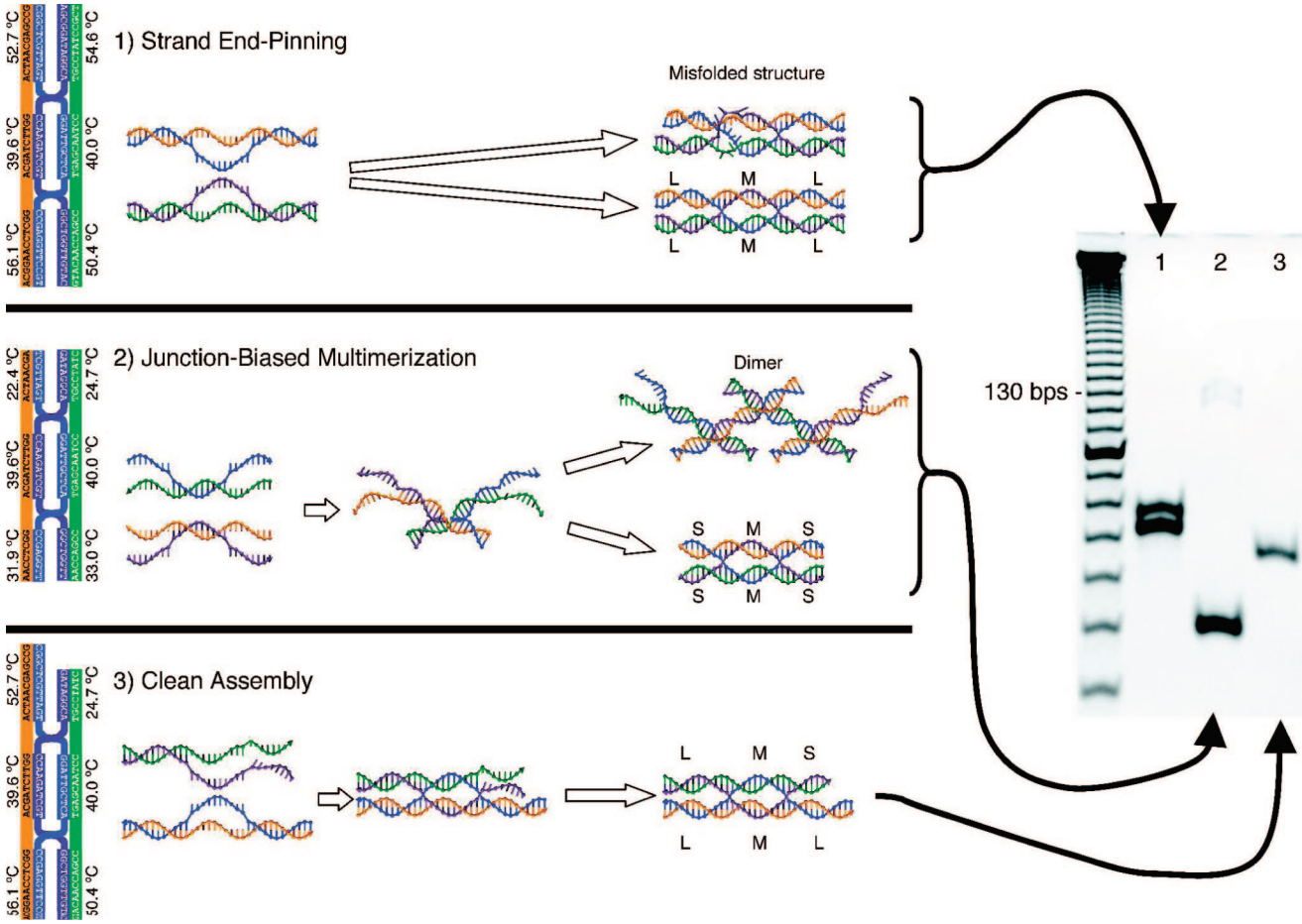

Figure 2. DP assembly success and failure. The three rows show three attempts to assemble DPE molecules. At the left side of each row is a sequence-structure diagram of the target molecule, with the sequences typed 5′ to 3′ and the indicated melting temperature of each segment as calculated by HyTher (version 1.0, Nicolas Peyret and John SantaLucia, Jr., Wayne State University).[68,69] From left to right across each row, structural models of the different states of the system are shown as it cools down while being annealed. At the right side of each row is the target molecule, with the relative lengths of the sections indicated (12 bps is long (L), 10 bps is medium (M), and 8 bps is short (S)). Above the targets in the first two rows is a possible failure product. The top row shows strand end-pinning, where the core cannot properly wind up because the arms have all hybridized first. The middle row shows junction-biased multimerization, where the preference of the Holliday junctions to form antiparallel structures resists proper folding to the target structure and promotes multimerization. The bottom row shows a successful assembly, where a combination of long and short arms direct the assembly to avoid the problems above. At right is a polyacrylamide gel of 20 pmoles of each tile, stained with ethidium bromide. The lowest band in each lane runs at approximately the expected rate for the target molecule. The left lane is a 10 bp reference ladder with a darker 100 bp band.

misfolding. Row 3 of Figure 2 shows an example of this. The target structure has three long arms, medium length core sections, and one short arm. As the system is annealed, the three long arms hybridize first. The lower subcomplex, with two long arms, is a cyclic structure that prevents junction-biased multimer formation before the junctions have assembled. The upper complex, with the 8 bp arm shorter than the core sections, prevents strand end-pinning. As the system cools, the two subcomplexes hybridize together as the core assembles, and finally, the short arm hybridizes. As can be seen from lane 3 of the gel, this assembly strategy works quite well, with neither multimers nor band splitting visible at the 1 μM concentrations that are typically used in the field.[5,10,70]

The top of Figure 3 shows a sequence-structure diagram of two DP tiles that have been designed to assemble into a planar array. On the right is a DPON. On the left is a DPOW* molecule, a DPOW that has a bulged hairpin loop attached[5] to one domain of its core. We have constructed both of these tiles, as well as the DPOW, using the same sequences but no hairpin loop. All of the DPO molecules we have constructed have had two long arms diagonally opposite each other to prevent junction-biased multimerization, with the other two arms short to prevent end-pinning and the core intermediate in length. The hairpin in the DPOW* is longer than the 8 bases typically used for this purpose. It has 11 bases, in the hopes that it will be very stable and will encourage winding of the core before the hybridization of the 10-base arms pin the strand ends. At the right of Figure 3 is a scan of a gel displaying formation of the DPON and DPOW molecules with neither multimerization nor band splitting. The right lane of the gel shows the end-pinned DPE band splitting for comparison.

When the array is assembled with DPOW tiles, it is relatively flat and featureless as seen in the lower left atomic force micrograph of Figure 3. At the usual 10 mM concentration of Mg^{2+} counterions, the starred array did not show stripes (data not shown). When the concentration was

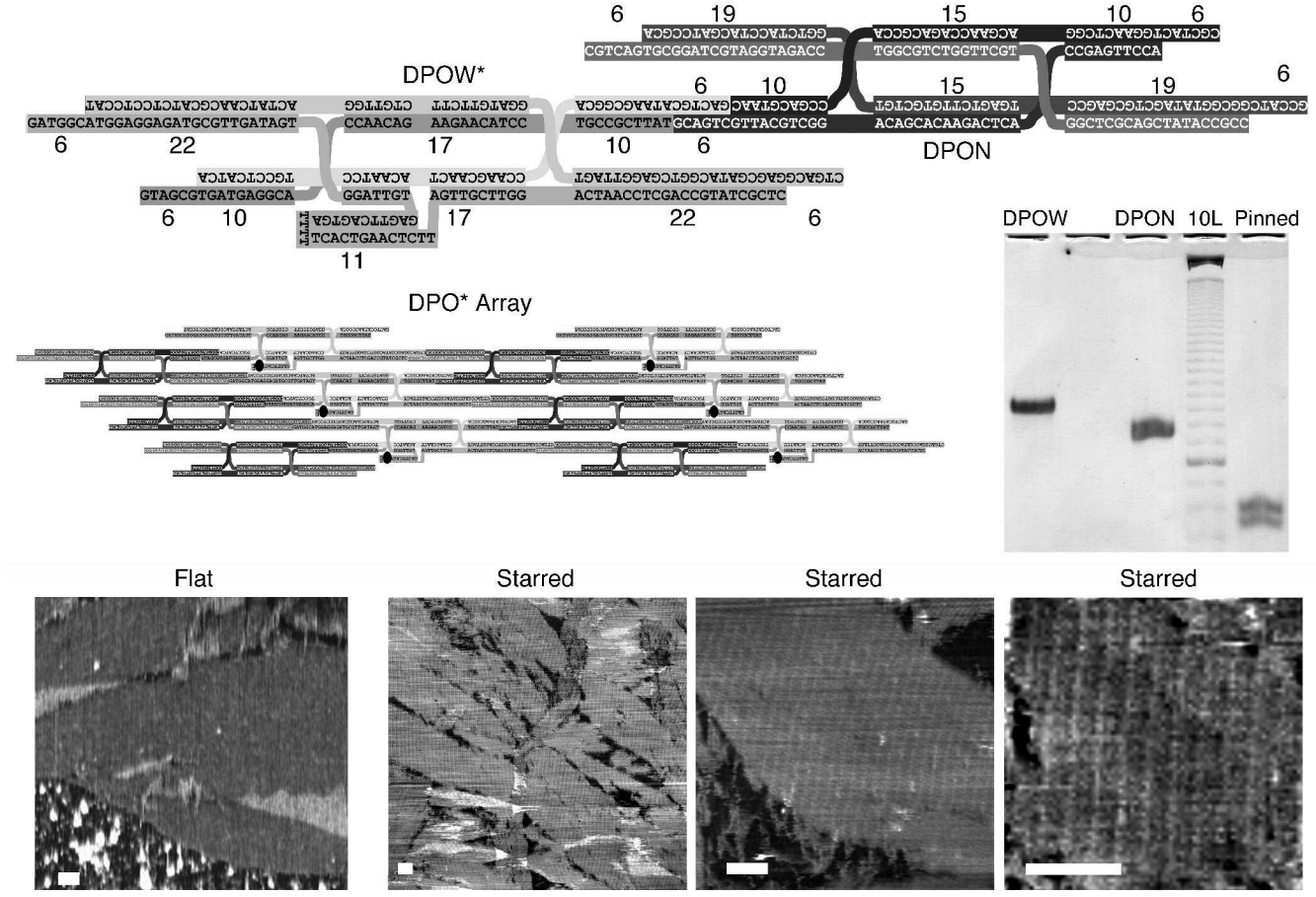

Figure 3. DPO tiles. At the top is a sequence-structure diagram of DPOW* and DPON tiles designed to form the array shown below. The sequences are typed 5′ to 3′, and the number of base pairs in each duplex domain is indicated. In the array diagram, the hairpin has been compressed and marked with a black oval. The stripes seen in the atomic force micrographs of the starred arrays are from the lines of black ovals slanting down to the right. The slopes and thus the distance between the lines are a function of the 105 bps between hairpins (35.7 nm) and the maximum separation between neighboring duplex domains (~2.4 nm).[31] At the right is a nondenaturing polyacrylamide gel showing 20 pmoles each of a DPOW (without the hairpin), a DPON, a 10 bp marker ladder with the 100 bp band darkened, and the end-pinned DPE from Figure 2 for comparison. The lowest band in each lane runs at approximately the speed of the target molecule. Along the bottom are micrographs of arrays taken in tapping mode in buffer with 4 nm z scales. At the left is a flat array of DPON and DPOW tiles. To the right are three starred arrays of DPON and DPOW* tiles, annealed in a 35 mM, concentration of Mg^{2+} counterions. All scale bars are 100 nm. The stripes on the starred arrays are expected roughly 27.7 nm apart but are observed 26.1 ± 0.8 nm apart.

increased to 35 mM, the stripes could be seen, as shown in the three panels on the lower right. As the sequence-structure diagram of the array indicates, the perpendicular distance between the stripes will depend both on the 105 base repeat length of the system and the vertical spacing of the duplex domains. If the domains were perfectly straight, the separation between stripes would be about 17 nm. However, the domains of DX (and DX-like) arrays are known to bend, presumably because of phosphate repulsion. Extrapolating from Rothemund's observations of domain separations[31] to our system with 8.5 turns of DNA between crossovers, we expect neighboring DNA domains to be approximately 2.4 nm apart at their widest separation, which would give stripes roughly 27.7 nm apart. We observed stripes 26.1 ± 0.8 nm apart, which is in reasonable agreement with the simple model.

On the left of Figure 4 is a sequence-structure diagram of a DPE array, with the arm lengths indicated. Tile A has a 10 base core; tile B an 11 base core, and both form cleanly, as can be seen on the gel at the right. Because there is not exactly one turn of DNA in the core of either of these tiles, they develop strain when forced into a planar array.[51] The micrographs in Figure 4 show that patches roughly 10 tiles wide form reasonably well, but the larger assemblies are somewhat wavy and prone to having numerous gaps. Note that this system has no hairpin star. The stripes in the micrographs appear to be lines of DXs. Attempts at forming starred arrays by adding a hairpin to an arm of tile B produced qualitatively similar arrays, with the hairpins not visible (data not shown).

It might seem an unwarranted approximation that the various sections of a DNA nanostructure will assemble at the same temperatures they would if they were hybridized disconnected from each other. Consider, for example, the green and purple strands in Figure 2, molecule 3. Once the 12 bp segment hybridizes, the 8 bp segment might be expected to seal up as well and create end-pinning problems. Yet no end-pinning is observed for this system. Fu and Seeman observed strong end-pinning effects when the outer arms and core of a DPE were all 10 bps but observed no

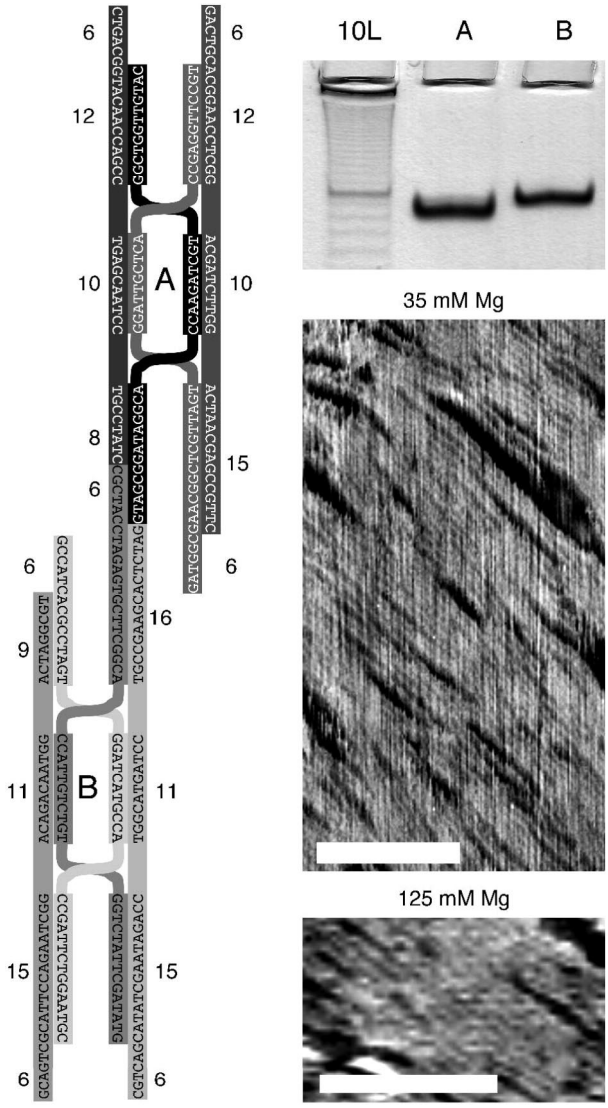

Figure 4. DPE arrays. At the left is a sequence-structure diagram of two DPE tiles that are designed to assemble into a planar array. The sequences are typed 5′ to 3′, and the number of base pairs in each duplex domain is indicated. Top, right is a nondenaturing polyacrylamide gel showing clean formation of the two tiles and a 10 bp marker ladder with the 100 bp band darkened. Below that are two atomic force micrographs of the assembled array taken in tapping mode in buffer with 4 nm z scales. The arrays were annealed in buffers with the indicated concentrations of Mg^{2+} counterions. Scale bars are 100 nm. The lines in the array appear to be rows of DX tiles, approximately 5.8 ± 0.7 nm apart.

end-pinning when the outer arms were even 1 base shorter.[4] So it appears that the effects of cooperativity are smaller than we might expect. Nevertheless, for intricate structures,[14,25,28,31,42] even assuming that the sections hybridize in a predictable order, we find it is not always possible to determine whether there will be end-pinning. Thus, there is no completely general algorithm that guarantees well-formed nanostructures in all cases. The best we can do is to provide some guidelines that, when they can be applied, should yield good structures: (1) Each element (arm or junction) that is going to be stressed during or after the assembly of a system should have at least one strand firmly fixed running through that element before the stress arises. (2)Structures should assemble in such a way that, as each section hybridizes, at least one end of one strand in that section is free to wind around the other strand.

Rule 1 avoids multimerization, which is a natural way for a system to avoid assembling into a stressed configuration. Note that in this context "firmly" refers to segments that are able to maintain their connections under the stress of the system. Rule 1 includes, as a special case, parallel Holliday junctions as stressed components in a system. For example, the core and junctions in a DPE molecule are stressed because they maintain the parallel state of the junctions. The blue and orange complex in Figure 2, molecule 3, has the strand ends fixed and at least one strand running through each section of the core and each of the junctions. This complex thus resists multimerization as the stress develops in the system when the green and purple complex hybridizes with it.

Rule 2 addresses the problem of end-pinning. One way to satisfy rule 2 is by designing the strands to hybridize sequentially either from one end to the other, or from the center out to the ends. In fact, not all strands need to follow this algorithm for a structure to satisfy rule 2. For example, the blue and orange strands in Figure 2, molecule 3, have their ends pinned before their central sections have hybridized. Nevertheless, the system satisfies rule 2 since the other strands in the core are unpinned when the core assembles.[52]

There are several lessons to be learned from the problems that stunted the development of DPs for the last fifteen years. Junction-biased misfolding arises when, at some temperature encountered during assembly, the difference in free energy between the correctly and the incorrectly folded states is small enough that a seemingly small bias can irreversibly shift a significant fraction of the molecular population into the wrong state. These problems can be minimized by careful design of assembly paths and the characterization of any system elements, such as novel junctions, DNAzymes, surfaces, nanoparticles, peptides, or other non-DNA elements that might bias the folding process.

Strand end-pinning is a deceptive problem that could potentially affect virtually any type of DNA nanostructure, including DAs. It should be noted that the end-pinned DPE in Figure 2 is virtually the smallest and simplest system where end-pinning is possible, and thus, the PAGE separation of the target and misfolded structures is at its largest. Yet these two bands are barely resolved. For a larger system with a similar problem, the target and misfolded states may not be distinguishable via conventional PAGE techniques. Further, hydroxyl radical autofootprinting may only be marginally useful in this regard for two reasons. First, it is likely that, for any given ensemble of test molecules, some will fold properly in spite of end-pinning, and thus, junction protection will be observed as expected. Second, end-pinned structures can misfold in a variety of ways, so even if no molecules fold properly, each junction may well show significant protection. Mismatch binding proteins[71] or potassium permanganate, which selectively reacts with unstacked thymine bases,[56,72] may be able to distinguish between the correctly and the incorrectly folded structures and provide

an important evaluation tool for suspect motifs. Fortunately, for the same reasons that end-pinning problems are hard to detect, they may make minimal disruptions in systems. There are likely some systems already in the literature that have end-pinning misfolds but function well regardless.

The clean assembly of DPs opens up possibilities for the rational design of numerous other DNA motifs. It should be possible to construct not just DPs but parallel triple-, quadruple-, and other crossovers just as their antiparallel versions were built.[8,25,30] It should also be possible to make numerous hybrids of DPs and DAs, just as DAs have been combined with PXs.[38,73] Construction of such a hybrid was reported as this manuscript was being written (for an application where a DP was desired, but deemed problematic).[73] DP-like elements can also be introduced into star motifs,[10–13] DNA origami,[31] DNA tubes,[17–19,22–25,27,52] and a host of other structures that have been based on DAs.[7–9,15,19,28–30]

In summary, we have presented an assembly pathway analysis for the design of DNA nanostructures that will join geometric modeling and sequence optimization as a basic design strategy for nucleic acid nanostructures. The key features of this approach are the consideration of end-pinning and junction-biasing effects on assembly. We have used this approach and knowledge of the structural bias of Holliday junctions to understand previously unexplained failures in DP assembly and to develop new designs that successfully formed representatives of all major classes of DP.

Acknowledgment. We are grateful to Oleg Gang, Daniel van der Lelie, the Center for Functional Nanomaterials and the Biology Department at Brookhaven National Laboratory for support and the use of their equipment. This research has been supported by Laboratory Directed Research and Development grant 07-025 from Brookhaven National Laboratory, and by the U.S. DOE Office of Science and Office of Basic Energy Sciences, under Contract No. DE-AC02-98CH10886.

Supporting Information Available: The design parameters used to generate the DNA base sequences, and the experimental methods. This material is available free of charge via the Internet at http://pubs.acs.org.

References

(1) Seeman, N. C. *J. Theor. Biol.* **1982**, *99*, 237–247.
(2) Kallenbach, N. R.; Ma, R. I.; Seeman, N. C. *Nature* **1983**, *305*, 829–831.
(3) Chen, J.; Seeman, N. C. *Nature* **1991**, *350*, 631–633.
(4) Fu, T. J.; Seeman, N. C. *Biochemistry* **1993**, *32*, 3211–3220.
(5) Winfree, E.; Liu, F.; Wenzler, L. A.; Seeman, N. C. *Nature* **1998**, *394*, 539–544.
(6) Mao, C. D.; Sun, W. Q.; Seeman, N. C. *J. Am. Chem. Soc.* **1999**, *121*, 5437–5443.
(7) Yang, X. P.; Wenzler, L. A.; Qi, J.; Li, X. J.; Seeman, N. C. *J. Am. Chem. Soc.* **1998**, *120*, 9779–9786.
(8) LaBean, T. H.; Yan, H.; Kopatsch, J.; Liu, F.; Winfree, E.; Reif, J. H.; Seeman, N. C. *J. Am. Chem. Soc.* **2000**, *122*, 1848–1860.
(9) Yan, H.; Seeman, N. C. *J. Supramol. Chem.* **2001**, *1*, 229–237.
(10) Yan, H.; Park, S. H.; Finkelstein, G.; Reif, J. H.; LaBean, T. H. *Science* **2003**, *301*, 1882–1884.
(11) He, Y.; Chen, Y.; Liu, H.; Ribbe, A. E.; Mao, C. *J. Am. Chem. Soc.* **2005**, *127*, 12202–12203.
(12) He, Y.; Mao, C. *Chem. Commun.* **2006**, 968–969.
(13) He, Y.; Ye, T.; Su, M.; Zhang, C.; Ribbe, A. E.; Jiang, W.; Mao, C. *Nature* **2008**, *452*, 198–201.
(14) Shih, W. M.; Quispe, J. D.; Joyce, G. F. *Nature* **2004**, *427*, 618–621.
(15) Chelyapov, N.; Brun, Y.; Gopalkrishnan, M.; Reishus, D.; Shaw, B.; Adleman, L. *J. Am. Chem. Soc.* **2004**, *126*, 13924–13925.
(16) Shen, Z. Y.; Yan, H.; Wang, T.; Seeman, N. C. *J. Am. Chem. Soc.* **2004**, *126*, 1666–1674.
(17) Mathieu, F.; Liao, S.; Kopatsch, J.; Wang, T.; Mao, C.; Seeman, N. C. *Nano Lett.* **2005**, *5*, 661–665.
(18) Park, S. H.; Barish, R.; Li, H.; Reif, J. H.; Finkelstein, G.; Yan, H.; LaBean, T. H. *Nano Lett.* **2005**, *5*, 693–696.
(19) Wei, B.; Mi, Y. *Biomacromolecules* **2005**, *6*, 2528–2532.
(20) He, Y.; Tian, Y.; Chen, Y.; Deng, Z.; Ribbe, A. E.; Mao, C. *Angew. Chem. Int. Ed* **2005**, *44*, 6694–6696.
(21) Erben, C. M.; Goodman, R. P.; Turberfield, A. J. *J. Am. Chem. Soc.* **2007**, *129*, 6992–6993.
(22) Douglas, S. M.; Chou, J. J.; Shih, W. M. *Proc. Natl. Acad. Sci.* **2007**, *104*, 6644–6648.
(23) Rothemund, P. W. K.; Ekani-Nkodo, A.; Papadakis, N.; Kumar, A.; Fygenson, D. K.; Winfree, E. *J. Am. Chem. Soc.* **2004**, *126*, 16344–16352.
(24) Mitchell, J. C.; Harris, J. R.; Malo, J.; Bath, J.; Turberfield, A. J. *J. Am. Chem. Soc.* **2004**, *126*, 16342–16343.
(25) Ke, Y.; Liu, Y.; Zhang, J.; Yan, H. *J. Am. Chem. Soc.* **2006**, *128*, 4414–4421.
(26) Goodman, R. P.; Schaap, I. A. T.; Tardin, C. F.; Erben, C. M.; Berry, R. M.; Schmidt, C. F.; Turberfield, A. J. *Science* **2005**, *310*, 1661–1665.
(27) Kuzuya, A.; Wang, R.; Sha, R.; Seeman, N. C. *Nano Lett.* **2007**, *7*, 1757–1763.
(28) Constantinou, P. E.; Wang, T.; Kopatsch, J.; Israel, L. B.; Zhang, X.; Ding, B.; Sherman, W. B.; Wang, X.; Zheng, J.; Sha, R.; Seeman, N. C. *Org. Biomol. Chem.* **2006**, *4*, 3414–3419.
(29) Ding, B.; Sha, R.; Seeman, N. C. *J. Am. Chem. Soc.* **2004**, *126*, 10230–10231.
(30) Reishus, D.; Shaw, B.; Brun, Y.; Chelyapov, N.; Adleman, L. *J. Am. Chem. Soc.* **2005**, *127*, 17590–17591.
(31) Rothemund, P. W. K. *Nature* **2006**, *440*, 297–302.
(32) Mao, C.; Sun, W.; Shen, Z.; Seeman, N. C. *Nature* **1999**, *397*, 144–146.
(33) Yurke, B.; Turberfield, A. J.; Mills, A. P.; Simmel, F. C.; Neumann, J. L. *Nature* **2000**, *406*, 605–608.
(34) Yan, H.; Zhang, X.; Shen, Z.; Seeman, N. C. *Nature* **2002**, *415*, 62–65.
(35) Feng, L.; Park, S. H.; Reif, J. H.; Yan, H. *Angew. Chem., Int. Ed. Engl.* **2003**, *42*, 4342–4346.
(36) Sherman, W. B.; Seeman, N. C. *Nano Lett.* **2004**, *4*, 1203–1207.
(37) Venkataraman, S.; Dirks, R. M.; Rothemund, P. W. K.; Winfree, E.; Pierce, N. A. *Nat. Nanotechnol.* **2007**, *2*, 490–494.
(38) Ding, B.; Seeman, N. C. *Science* **2006**, *314*, 1583−1585.
(39) Dittmer, W. U.; Reuter, A.; Simmel, F. C. *Angew. Chem., Int. Ed. Engl.* **2004**, *43*, 3550–3553.
(40) Friedrichs, E.; Simmel, F. C. *Chembiochem* **2007**, *8*, 1662–1666.
(41) Mao, C.; LaBean, T. H.; Reif, J. H.; Seeman, N. C. *Nature* **2000**, *407*, 493–496.
(42) Sa-Ardyen, P.; Jonoska, N.; Seeman, N. C. *J. Am. Chem. Soc.* **2004**, *126*, 6648–6657.
(43) Rothemund, P. W. K.; Papadakis, N.; Winfree, E. *Plos Biology* **2004**, *2*, 2041–2053.
(44) Xiao, S.; Liu, F.; Rosen, A. E.; Hainfeld, J. F.; Seeman, N. C.; Musier-Forsyth, K.; Kiehl, R. A. *Journal of Nanoparticle Research* **2002**, *4*, 313–317.
(45) Zheng, J. W.; Constantinou, P. E.; Micheel, C.; Alivisatos, A. P.; Kiehl, R. A.; Seeman, N. C. *Nano Letters* **2006**, *6*, 1502–1504.
(46) Sharma, J.; Chhabra, R.; Liu, Y.; Ke, Y.; Yan, H. *Angew. Chem., Int. Ed. Engl.* **2006**, *45*, 730–735.
(47) Lin, C.; Katilius, E.; Liu, Y.; Zhang, J.; Yan, H. *Angew. Chem., Int. Ed. Engl.* **2006**, *45*, 5296–5301.
(48) Malo, J.; Mitchell, J. C.; Venien-Bryan, C.; Harris, J. R.; Wille, H.; Sherratt, D. J.; Turberfield, A. J. *Angew. Chem., Int. Ed.* **2005**, *44*, 3057–3061.
(49) Song, C.; Chen, Y. Q.; Xiao, S. J.; Ba, L.; Gu, Z. Z.; Pan, Y.; You, X. Z. *Chem. Mater.* **2005**, *17*, 6521–6524.
(50) Seeman, N. C. *J. Biomol. Struct. Dynamics* **1988**, *5*, 997–1004.
(51) Birac, J. J.; Sherman, W. B.; Kopatsch, J.; Constantinou, P. E.; Seeman, N. C. *J. Mol. Graph. Model.* **2006**, *25*, 470–480.
(52) Sherman, W. B.; Seeman, N. C. *Biophys. J.* **2006**, *90*, 4546–4557.
(53) Holliday, R. *Genet. Res.* **1964**, *5*, 282–304.

(54) Fu, T. J.; Tse-Dinh, Y. C.; Seeman, N. C. *J. Mol. Biol.* **1994**, *236*, 91–105.
(55) Fu, T. J.; Kemper, B.; Seeman, N. C. *Biochemistry* **1994**, *33*, 3896–3905.
(56) Sun, W. Q.; Mao, C. D.; Iwasaki, H.; Kemper, B.; Seeman, N. C. *J. Mol. Biol.* **1999**, *294*, 683–699.
(57) Wu, L.; Hickson, I. D. *Nature* **2003**, *426*, 870–874.
(58) Wu, L.; Chan, K. L.; Ralf, C.; Bernstein, D. A.; Garcia, P. L.; Bohr, V. A.; Vindigni, A.; Janscak, P.; Keck, J. L.; Hickson, I. D. *EMBO J.* **2005**, *24*, 2679–2687.
(59) Wu, L.; Bachrati, C. Z.; Ou, J. W.; Xu, C.; Yin, J. H.; Chang, M.; Wang, W. D.; Li, L.; Brown, G. W.; Hickson, I. D. *Proc. Natl. Acad. Sci. U.S.A.* **2006**, *103*, 4068–4073.
(60) Macris, M. A.; Krejci, L.; Bussen, W.; Shimamoto, A.; Sung, P. *DNA Repair* **2006**, *5*, 172–180.
(61) Raynard, S.; Bussen, W.; Sung, P. *J. Biol. Chem.* **2006**, *281*, 13861–13864.
(62) Bussen, W.; Raynard, S.; Busygina, V.; Singh, A. K.; Sung, P. *J. Biol. Chem.* **2007**, *282*, 31484–31492.
(63) Murchie, A. I. H.; Clegg, R. M.; von Kitzing, E.; Duckett, D. R.; Diekmann, S.; Lilley, D. M. J. *Nature* **1989**, *341*, 763–766.
(64) Watson, J.; Hays, F. A.; Ho, P. S. *Nucleic Acids Res.* **2004**, *32*, 3017–3027.
(65) Seeman, N. C. *Synlett* **2000**, *2000*, 1536–1548.
(66) Israel-Dreilinger, L. B. Ph.D. Thesis, New York University, New York, 2006.
(67) Dirks, R. M.; Bois, J. S.; Schaeffer, J. M.; Winfree, E.; Pierce, N. A. *SIAM Rev* **2007**, *49*, 65–88.
(68) SantaLucia, J., Jr. *Proc. Natl. Acad. Sci.* **1998**, *95*, 1460–1465.
(69) Peyret, N.; Seneviratne, P. A.; Allawi, H. T.; SantaLucia, J., Jr. *Biochemistry* **1999**, *38*, 3468–3477.
(70) Muller, B. K.; Reuter, A.; Simmel, F. C.; Lamb, D. C. *Nano Lett.* **2006**, *6*, 2814–2820.
(71) Kunkel, T. A.; Erie, D. A. *Annu. Rev. Biochem.* **2005**, *74*, 681–710.
(72) Kvaratskhelia, M.; Budihas, S. R.; Le Grice, S. F. J. *J. Biol. Chem.* **2002**, *277*, 16689–16696.
(73) Liu, W.; Wang, X.; Wang, T.; Sha, R.; Seeman, N. C. *Nano Lett.* **2008**, *8*, 317–322.

NL800907Y